Eur. Phys. J. C 38, 437–445 (2005)
Digital Object Identifier (DOI) 10.1140/epjc/s2004-02085-x

THE EUROPEAN PHYSICAL JOURNAL C

Measurement of prompt photon cross sections in photoproduction at HERA

The H1 Collaboration

A. Aktas[10], V. Andreev[26], T. Anthonis[4], A. Asmone[33], A. Babaev[25], S. Backovic[37], J. Bähr[37], P. Baranov[26], E. Barrelet[30], W. Bartel[10], S. Baumgartner[38], J. Becker[39], M. Beckingham[21], O. Behnke[13], O. Behrendt[7], A. Belousov[26], Ch. Berger[1], N. Berger[38], T. Berndt[14], J.C. Bizot[28], J. Böhme[10], M.-O. Boenig[7], V. Boudry[29], J. Bracinik[27], V. Brisson[28], H.-B. Bröker[2], D.P. Brown[10], D. Bruncko[16], F.W. Büsser[11], A. Bunyatyan[12,36], G. Buschhorn[27], L. Bystritskaya[25], A.J. Campbell[10], S. Caron[1], F. Cassol-Brunner[22], K. Cerny[32], V. Chekelian[27], C. Collard[4], J.G. Contreras[23], Y.R. Coppens[3], J.A. Coughlan[5], B.E. Cox[21], G. Cozzika[9], J. Cvach[31], J.B. Dainton[18], W.D. Dau[15], K. Daum[35,41], B. Delcourt[28], R. Demirchyan[36], A. De Roeck[10,44], K. Desch[11], E.A. De Wolf[4], C. Diaconu[22], J. Dingfelder[13], V. Dodonov[12], A. Dubak[27], C. Duprel[2], G. Eckerlin[10], V. Efremenko[25], S. Egli[34], R. Eichler[34], F. Eisele[13], M. Ellerbrock[13], E. Elsen[10], M. Erdmann[10,42], W. Erdmann[38], P.J.W. Faulkner[3], L. Favart[4], A. Fedotov[25], R. Felst[10], J. Ferencei[10], M. Fleischer[10], P. Fleischmann[10], Y.H. Fleming[10], G. Flucke[10], G. Flügge[2], A. Fomenko[26], I. Foresti[39], J. Formánek[32], G. Franke[10], G. Frising[1], E. Gabathuler[18], K. Gabathuler[34], E. Garutti[10], J. Garvey[3], J. Gayler[10], R. Gerhards[10,†], C. Gerlich[13], S. Ghazaryan[36], L. Goerlich[6], N. Gogitidze[26], S. Gorbounov[37], C. Grab[38], H. Grässler[2], T. Greenshaw[18], M. Gregori[19], G. Grindhammer[27], C. Gwilliam[21], D. Haidt[10], L. Hajduk[6], J. Haller[13], M. Hansson[20], G. Heinzelmann[11], R.C.W. Henderson[17], H. Henschel[37], O. Henshaw[3], R. Heremans[4], G. Herrera[24], I. Herynek[31], R.-D. Heuer[11], M. Hildebrandt[34], K.H. Hiller[37], J. Hladký[31], P. Höting[2], D. Hoffmann[22], R. Horisberger[34], A. Hovhannisyan[36], M. Ibbotson[21], M. Ismail[21], M. Jacquet[28], L. Janauschek[27], X. Janssen[10], V. Jemanov[11], L. Jönsson[20], D.P. Johnson[4], H. Jung[20,10], D. Kant[19], M. Kapichine[8], M. Karlsson[20], J. Katzy[10], N. Keller[39], J. Kennedy[18], I.R. Kenyon[3], C. Kiesling[27], M. Klein[37], C. Kleinwort[10], T. Kluge[1], G. Knies[10], A. Knutsson[20], B. Koblitz[27], V. Korbel[10], P. Kostka[37], R. Koutouev[12], A. Kropivnitskaya[25], J. Kroseberg[39], J. Kückens[10], T. Kuhr[10], M.P.J. Landon[19], W. Lange[37], T. Laštovička[37,32], P. Laycock[18], A. Lebedev[26], B. Leißner[1], R. Lemrani[10], V. Lendermann[14], S. Levonian[10], L. Lindfeld[39], K. Lipka[37], B. List[38], E. Lobodzinska[37,6], N. Loktionova[26], R. Lopez-Fernandez[10], V. Lubimov[25], H. Lueders[11], D. Lüke[7,10], T. Lux[11], L. Lytkin[12], A. Makankine[8], N. Malden[21], E. Malinovski[26], S. Mangano[38], P. Marage[4], J. Marks[13], R. Marshall[21], M. Martisikova[10], H.-U. Martyn[1], S.J. Maxfield[18], D. Meer[38], A. Mehta[18], K. Meier[14], A.B. Meyer[11], H. Meyer[35], J. Meyer[10], S. Michine[26], S. Mikocki[6], I. Milcewicz-Mika[6], D. Milstead[18], A. Mohamed[18], F. Moreau[29], A. Morozov[8], I. Morozov[8], J.V. Morris[5], M.U. Mozer[13], K. Müller[39], P. Murín[16,43], V. Nagovizin[25], B. Naroska[11], J. Naumann[7], Th. Naumann[37], P.R. Newman[3], C. Niebuhr[10], A. Nikiforov[27], D. Nikitin[8], G. Nowak[6], M. Nozicka[32], R. Oganezov[36], B. Olivier[10], J.E. Olsson[10], G.Ossoskov[8], D. Ozerov[25], C. Pascaud[28], G.D. Patel[18], M. Peez[29], E. Perez[9], A. Perieanu[10], A. Petrukhin[25], D. Pitzl[10], R. Plačakytė[27], R. Pöschl[10], B. Portheault[28], B. Povh[12], N. Raicevic[37], Z. Ratiani[10], P. Reimer[31], B. Reisert[27], A. Rimmer[18], C. Risler[27], E. Rizvi[3], P. Robmann[39], B. Roland[4], R. Roosen[4], A. Rostovtsev[25], Z. Rurikova[27], S. Rusakov[26], K. Rybicki[6,†], D.P.C. Sankey[5], E. Sauvan[22], S. Schätzel[13], J. Scheins[10], F.-P. Schilling[10], P. Schleper[10], S. Schmidt[27], S. Schmitt[39], M. Schneider[22], L. Schoeffel[9], A. Schöning[38], V. Schröder[10], H.-C. Schultz-Coulon[14], C. Schwanenberger[10], K. Sedlák[31], F. Sefkow[10], I. Sheviakov[26], L.N. Shtarkov[26], Y. Sirois[29], T. Sloan[17], P. Smirnov[26], Y. Soloviev[26], D. South[10], V. Spaskov[8], A. Specka[29], H. Spitzer[11], R. Stamen[10], B. Stella[33], J. Stiewe[14], I. Strauch[10], U. Straumann[39], V. Tchoulakov[8], G. Thompson[19], P.D. Thompson[3], F. Tomasz[14], D. Traynor[19], P. Truöl[39], G. Tsipolitis[10,40], I. Tsurin[37], J. Turnau[6], E. Tzamariudaki[27], A. Uraev[25], M. Urban[39], A. Usik[26], D. Utkin[25], S. Valkár[32], A. Valkárová[32], C. Vallée[22], P. Van Mechelen[4], A. Vargas Trevino[7], Y. Vazdik[26], C. Veelken[18], A. Vest[1], S. Vinokurova[10], V. Volchinski[36], K. Wacker[7], J. Wagner[10], G. Weber[11], R. Weber[38], D. Wegener[7], C. Werner[13], N. Werner[39], M. Wessels[1], B. Wessling[11], G.-G. Winter[10], Ch. Wissing[7], E.-E. Woehrling[3], R. Wolf[13], E. Wünsch[10], S. Xella[39], W. Yan[10], J. Žáček[32], J. Zálešák[32], Z. Zhang[28], A. Zhokin[25], H. Zohrabyan[36], F. Zomer[28]

[1] I. Physikalisches Institut der RWTH, Aachen, Germany[a]
[2] III. Physikalisches Institut der RWTH, Aachen, Germany[a]
[3] School of Physics and Astronomy, University of Birmingham, Birmingham, UK[b]
[4] Inter-University Institute for High Energies ULB-VUB, Brussels; Universiteit Antwerpen, Antwerpen; Belgium[c]
[5] Rutherford Appleton Laboratory, Chilton, Didcot, UK[b]
[6] Institute for Nuclear Physics, Cracow, Poland[d]

[7] Institut für Physik, Universität Dortmund, Dortmund, Germany[a]
[8] Joint Institute for Nuclear Research, Dubna, Russia
[9] CEA, DSM/DAPNIA, CE-Saclay, Gif-sur-Yvette, France
[10] DESY, Hamburg, Germany
[11] Institut für Experimentalphysik, Universität Hamburg, Hamburg, Germany[a]
[12] Max-Planck-Institut für Kernphysik, Heidelberg, Germany
[13] Physikalisches Institut, Universität Heidelberg, Heidelberg, Germany[a]
[14] Kirchhoff-Institut für Physik, Universität Heidelberg, Heidelberg, Germany[a]
[15] Institut für experimentelle und Angewandte Physik, Universität Kiel, Kiel, Germany
[16] Institute of Experimental Physics, Slovak Academy of Sciences, Košice, Slovak Republic[e,f]
[17] Department of Physics, University of Lancaster, Lancaster, UK[b]
[18] Department of Physics, University of Liverpool, Liverpool, UK[b]
[19] Queen Mary and Westfield College, London, UK[b]
[20] Physics Department, University of Lund, Lund, Sweden[g]
[21] Physics Department, University of Manchester, Manchester, UK[b]
[22] CPPM, CNRS/IN2P3 - Univ Mediterranee, Marseille - France
[23] Departamento de Fisica Aplicada, CINVESTAV, Mérida, Yucatán, México[k]
[24] Departamento de Fisica, CINVESTAV, México[k]
[25] Institute for Theoretical and Experimental Physics, Moscow, Russia[l]
[26] Lebedev Physical Institute, Moscow, Russia[e]
[27] Max-Planck-Institut für Physik, München, Germany
[28] LAL, Université de Paris-Sud, IN2P3-CNRS, Orsay, France
[29] LLR, Ecole Polytechnique, IN2P3-CNRS, Palaiseau, France
[30] LPNHE, Universités Paris VI and VII, IN2P3-CNRS, Paris, France
[31] Institute of Physics, Academy of Sciences of the Czech Republic, Praha, Czech Republic[e,i]
[32] Faculty of Mathematics and Physics, Charles University, Praha, Czech Republic[e,i]
[33] Dipartimento di Fisica Università di Roma Tre and INFN Roma 3, Roma, Italy
[34] Paul Scherrer Institut, Villigen, Switzerland
[35] Fachbereich Physik, Bergische Universität Gesamthochschule Wuppertal, Wuppertal, Germany
[36] Yerevan Physics Institute, Yerevan, Armenia
[37] DESY, Zeuthen, Germany
[38] Institut für Teilchenphysik, ETH, Zürich, Switzerland[j]
[39] Physik-Institut der Universität Zürich, Zürich, Switzerland[j]
[40] Also at Physics Department, National Technical University, Zografou Campus, 15773 Athens, Greece
[41] Also at Rechenzentrum, Bergische Universität Gesamthochschule Wuppertal, Germany
[42] Also at Institut für Experimentelle Kernphysik, Universität Karlsruhe, Karlsruhe, Germany
[43] Also at University of P.J. Šafárik, Košice, Slovak Republic
[44] Also at CERN, Geneva, Switzerland

Received: 13 July 2004 / Revised version: 15 November 2004 /
Published online: 17 December 2004 – © Springer-Verlag / Società Italiana di Fisica 2004

Abstract. Results are presented on the photoproduction of isolated prompt photons, inclusively and associated with jets, in the γp center of mass energy range $142 < W < 266\,\mathrm{GeV}$. The cross sections are measured for the transverse momentum range of the photons $5 < E_T^\gamma < 10\,\mathrm{GeV}$ and for associated jets with $E_T^{\mathrm{jet}} > 4.5\,\mathrm{GeV}$. They are measured differentially as a function of E_T^γ, E_T^{jet}, the pseudorapidities η^γ and η^{jet} and estimators of the momentum fractions x_γ and x_p of the incident photon and proton carried by the constituents participating in the hard process. In order to further investigate the underlying dynamics, the angular correlation between the prompt photon and the jet in the transverse plane is studied. Predictions by perturbative QCD calculations in next to leading order are about 30% below the inclusive prompt photon data after corrections for hadronisation and multiple interactions, but are in reasonable agreement with the results for prompt photons associated with jets. Comparisons with the predictions of the event generators PYTHIA and HERWIG are also presented.

[a] Supported by the Bundesministerium für Bildung und Forschung, FRG, under contract numbers 05 H1 1GUA /1, 05 H1 1PAA /1, 05 H1 1PAB /9, 05 H1 1PEA /6, 05 H1 1VHA /7 and 05 H1 1VHB /5
[b] Supported by the UK Particle Physics and Astronomy Research Council, and formerly by the UK Science and Engineering Research Council
[c] Supported by FNRS-FWO-Vlaanderen, IISN-IIKW and IWT and by Interuniversity Attraction Poles Programme, Belgian Science Policy
[d] Partially Supported by the Polish State Committee for Scientific Research, SPUB/DESY/P003/DZ 118/2003/2005

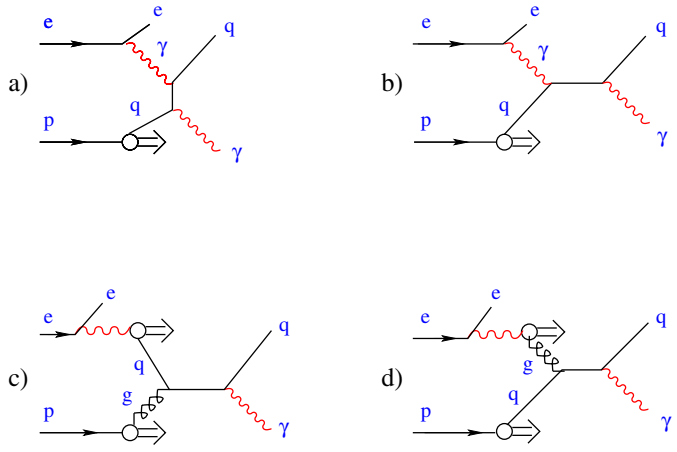

Fig. 1a–d. Examples of leading order diagrams producing prompt photons. **a**,**b** Direct photon interactions and **c**,**d** resolved photon interactions

1 Introduction

Prompt photon emission in hadronic interactions is a sensitive probe of QCD dynamics and partonic structure, providing complementary information to the study of jet production. Although cross sections are smaller in the prompt photon case, an isolated photon at large transverse energy E_T^γ can be related directly to the partonic event structure. This contrasts with jet measurements, where the partonic structure is obscured by the non-perturbative hadronisation process. Furthermore, experimental uncertainties associated with the transverse energy measurement are smaller for the electromagnetic showers initiated by photons than for the measurement of jets of hadrons. This paper presents results from the H1 experiment at HERA on the photoproduction of isolated prompt photons, both inclusively and in association with a jet. Here photons are called "prompt" if they are coupled to the interacting quarks (see Fig. 1), in contrast to photons which are produced as decay products of hadronic particles.

Next to leading order (NLO) perturbative QCD (pQCD) calculations have proved broadly successful in reproducing measured jet production rates from various colliders, provided hadronisation corrections are applied. In contrast, discrepancies have been observed between data on prompt photon production and NLO pQCD calculations in pp, $\bar{p}p$, pN (see e.g. [1]) and in γp [2] interactions. These discrepancies can be reduced by introducing intrinsic transverse momentum k_T to the incoming partons of the proton [1,3] or by soft gluon resummations [4]. NLO pQCD calculations of prompt photon production in photoproduction [5–9] are available, in which the incident photon interacts with the partons of the proton either directly (Fig. 1a,b) or via its "resolved" partonic structure (Fig. 1c,d). This paper investigates the extent to which fixed order NLO calculations are able to describe the new data. The data are also compared with the predictions of the event generators PYTHIA [10] and HERWIG [11] and with data on inclusive prompt photon production from the ZEUS collaboration [2].

2 Strategy of prompt photon measurement

The photoproduction process is initiated by quasi-real photons, which are produced in small angle ep scattering, where the scattered electron[1] escapes into the beam pipe. The requirement of a significant energy loss in the electron beam direction, together with the condition that no electrons are found in the selected events, suppresses contributions from neutral current (NC) deep inelastic scattering (DIS).

Photons are identified in the H1 liquid argon (LAr) calorimeter [12] as compact electromagnetic clusters with no track associated to them. The main experimental difficulty is the separation of the prompt photons from hadronic backgrounds, in particular π^0 meson decays, since at high energy the decay photons cannot be reconstructed separately in the calorimeter. Since the π^0 mesons are predominantly produced in jets, this background is strongly reduced by requiring the photon candidates to be isolated from other particles.

After the selection cuts described below, the π^0 background is still of similar size to the prompt photon signal. To extract the signal, different shower shape variables are combined to form a discriminator function which is fitted with a sum of contributions from simulated photons, π^0 and η mesons. The fit is done double-differentially in bins of transverse energy E_T^γ and pseudorapidity η^γ. [2]

The number of selected prompt photon events is corrected for detector effects by detailed simulations of prompt photon production in the H1 detector, using the event generators PYTHIA and HERWIG.

3 Event selection

The data were collected in the years 1996–2000 with the H1 detector [13] at HERA in data taking periods where electrons or positrons with energy $E_e = 27.6\,\text{GeV}$ collided with protons of energies $E_p = 820\,\text{GeV}$ or $E_p = 920\,\text{GeV}$. The data correspond to an integrated luminosity of $105\,\text{pb}^{-1}$

[e] Supported by the Deutsche Forschungsgemeinschaft
[f] Supported by VEGA SR grant no. 2/1169/2001
[g] Supported by the Swedish Natural Science Research Council
[i] Supported by the Ministry of Education of the Czech Republic under the projects INGO-LA116/2000 and LN00A006, by GAUK grant no 173/2000
[j] Supported by the Swiss National Science Foundation
[k] Supported by CONACYT, México, grant 400073-F
[l] Partially Supported by Russian Foundation for Basic Research, grant no. 00-15-96584
[†] Deceased

[1] The term "electron" is used for both electrons and positrons.
[2] The pseudorapidity η of an object with polar angle θ is given by $\eta = -\ln\,\tan(\theta/2)$, where θ is measured with respect to the z axis given by the proton beam direction. Transverse energies are also measured with respect to this axis unless otherwise specified.

of which $28.8\,\mathrm{pb}^{-1}$ and $61.3\,\mathrm{pb}^{-1}$ were recorded in e^+p interactions at center of mass energies $\sqrt{s} = 301\,\mathrm{GeV}$ and $\sqrt{s} = 319\,\mathrm{GeV}$, respectively, and $14.9\,\mathrm{pb}^{-1}$ were recorded in e^-p interactions at $\sqrt{s} = 319\,\mathrm{GeV}$.

The events are triggered by compact energy depositions in the LAr calorimeter, consistent with electron or photon showers. The trigger efficiency is $\approx 60\%$ at photon energies of 5 GeV, reaching 100% at $\approx 12\,\mathrm{GeV}$, as determined from NC events using a monitor trigger with a lower energy threshold [14].

The main requirements for the event selection are the following [14].

- A compact electromagnetic energy cluster, consistent with a γ shower, is reconstructed in the LAr calorimeter in the range $-1 < \eta^\gamma < 0.9$ and $E_T^\gamma > 5\,\mathrm{GeV}$. For the data at $\sqrt{s} = 301\,\mathrm{GeV}$ a threshold $E_T^\gamma > 7\,\mathrm{GeV}$ is required.[3] The η^γ range corresponds to the central barrel region of the LAr calorimeter [12].
- No track is allowed to point to this cluster within a distance of 25 cm in the plane transverse to the track at the calorimeter surface.
- Events with electron candidates in the LAr calorimeter or in the backward calorimeter SPACAL [15] are rejected. This restricts the virtuality of the exchanged photon to $Q^2 < 1\,\mathrm{GeV}^2$ and suppresses contributions from radiative DIS and QED Compton processes.
- At least two tracks are required in the central tracker [13, 16], which covers the angular range $20^\circ < \theta < 160^\circ$. This cut assures good reconstruction of the event vertex, which is required to be within ± 35 cm in z of the nominal vertex position.
- The inelasticity $y = W^2/s$, where W is the γp center of mass energy, is evaluated as $y = \sum (E - p_z)/2E_e$. Here the sum runs over all detected final state particles. The required range $0.2 < y < 0.7$ corresponds to $142 < W < 266\,\mathrm{GeV}$ for $E_p = 920\,\mathrm{GeV}$. The cut at high y reduces NC DIS background. The cut at low y removes beam gas background.
- The γ candidate is required to be isolated. The transverse energy, E_T^{cone}, in a cone around the γ candidate, given by distances below 1 unit in the $(\eta - \phi)$ plane, is required to be less than 10% of E_T^γ . A further cut to remove non-prompt photon background is based on the shower shape, as described in Sect. 4.
- Associated jets are reconstructed using the inclusive k_T algorithm [17] with a distance parameter $D = 1$ in the $(\eta - \phi)$ plane. The jets are selected in the jet energy and pseudorapidity ranges $E_T^{\mathrm{jet}} > 4.5\,\mathrm{GeV}$ and $-1 < \eta^{\mathrm{jet}} < 2.3$, respectively. If more than one jet is found, only the jet with the highest E_T^{jet} is considered.

4 Signal extraction

The prompt photon signal is extracted using a shower shape analysis based on the expectation that showers initiated by photons are typically narrower than π^0 or η initiated showers, with less energy deposited in the first calorimetric layer on average. This procedure exploits the fine segmentation of the electromagnetic section of the LAr calorimeter, which has transverse cell sizes varying between about $5 \times 7\,\mathrm{cm}^2$ and $7 \times 13\,\mathrm{cm}^2$ in the central barrel region. This part of the calorimeter has three layers in depth, corresponding to ≈ 20 radiation lengths. The first layer has a thickness of about 3 radiation lengths.

Three observables are used to discriminate against background. The mean transverse shower radius is given by $R = \sum_i r_i \varepsilon_i / \sum_i \varepsilon_i$, where r_i is the transverse distance of cell i with energy density ε_i measured with respect to the axis from the event vertex to the center of gravity of the γ candidate cluster. The shower hot core fraction (HCF) is the largest energy fraction of the candidate shower which is contained in 4 or 8 contiguous cells (depending on the calorimeter granularity) including the cell of highest energy. Finally the first layer fraction (FLF) is the energy fraction of the shower contained in the first, i.e. closest to the beam, layer of cells of the calorimeter. The observables R and FLF are expected to be smaller and HCF to be larger for the prompt photon showers than for background showers.

To discriminate between photon and background showers, probability densities for the three observables R, HCF and FLF are determined by simulation of photons and π^0 mesons [14]. The products of these three densities are used as likelihood functions. For each measured event a discriminator (d) is formed by the likelihood for photons divided by the sum of the likelihoods for photons and π^0 mesons. The discriminator d produces larger values for prompt photons than for the two-photon decays of π^0 mesons or the neutral decays of η mesons. This can be seen in Fig. 2a, where the measured distribution of d is shown together with the prediction of the PYTHIA Monte Carlo simulation, for which a common normalisation factor is applied to the sum of the prompt photon and background contributions. The lowest bin in Fig. 2a contains mostly background ($\approx 90\%$) which is composed of 65% π^0, 30% η and 5% other particles. After a cut $d > 0.125$, the remaining background ($\approx 50\%$) is composed of 94% π^0, 5% η and about 1% other particles. Figure 2a shows that the distribution in the discriminator d of signal plus background is well described by PYTHIA.

The contribution of prompt photons is determined by maximum likelihood fits of simulated photon, π^0 and η meson discriminator distributions to the data distribution for $d > 0.125$. Each measurement presented in Sect. 6 is obtained by summing the results of such fits performed independently in 6×6 bins of η^γ and E_T^γ. In this procedure, only the η/π^0 ratio (on average 5% after the selection requirements) is taken from PYTHIA.

The measured distributions of R, HCF and FLF for the full η^γ and E_T^γ range are shown in Fig. 2b-d together with the contributions of photons and π^0 and η background, the normalisations of which are taken from the fits to the discriminator distributions described above. The data distribution is well described by the extracted signal and back-

[3] The data at $\sqrt{s} = 301\,\mathrm{GeV}$ were taken prior to the upgrade of the LAr electronics, after which lower trigger thresholds became possible.

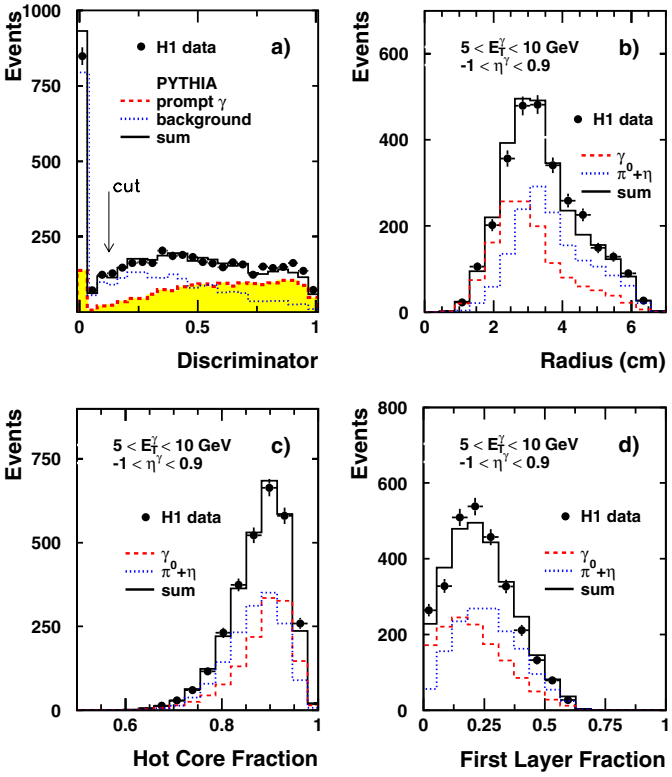

Fig. 2. a Distribution in the discriminator d, with the analysis cut indicated, for data (solid points), and PYTHIA normalised to the data (solid line), with prompt photons (dashed) and the sum of the background contributions (dotted). **b–d** Distributions of the mean transverse shower radius R, the hot core fraction HCF and the first layer fraction FLF for all selected photon candidates (data points). The contributions determined for photons (dashed lines), background ($\pi^0 + \eta$, dotted lines) and the sum (solid lines) are also shown

ground components. The discrimination between signal and background becomes weaker at high E_T^γ , where the R and HCF distributions of π^0 mesons and photons become more similar to each other. Therefore events with $E_T^\gamma > 10\,\text{GeV}$ are not included in the results presented below.

5 Monte Carlo generators and corrections to the data

The event generators PYTHIA [10] and HERWIG [11] are used [4] to correct the observed event yields for apparatus effects by means of a full simulation of the H1 detector. The average corrections from the two generators are applied. Both generators are based on leading order (LO) QCD matrix elements and leading log parton showers. Hadronisation is provided in PYTHIA by Lund string fragmentation [18] and in HERWIG by the decay of colourless parton clusters. Both generators model additional soft remnant-remnant interactions, termed multiple parton interactions (m.i.) in the following. The GRV(LO) [19] parton densities are used for the photon and the proton. In contrast to HERWIG, PYTHIA simulates radiation of photons from the electron line and photon production via fragmentation of final state quarks and gluons in di-jet events. In PYTHIA the parameter describing the intrinsic k_T of initial state partons in the proton is $k_0 = 1\,\text{GeV}$ (default) leading to $< k_T >= 0.9\,\text{GeV}$. HERWIG predictions are shown for the default value $k_T = 0$.

A correction factor of about 1.04 is applied to the $\sqrt{s} = 301\,\text{GeV}$ data in order to combine with the data at $\sqrt{s} = 319\,\text{GeV}$. The final results are presented for $\sqrt{s} = 319\,\text{GeV}$. Background from DIS events where the scattered electron fakes the prompt photon signatures due to tracker inefficiency leads to a subtraction of 3% in the lowest η^γ bin at high E_T^γ , and is negligible otherwise. Following the selection criteria described in Sect. 3, other sources of background are negligible.

6 Systematic uncertainties

The following sources of systematic errors are considered.

- The dominant systematic errors are due to possible imperfections in the simulation of the shower shapes. The quality of the simulated distributions of R, HCF and FLF is tested by comparing simulations of electrons with electron candidates from NC DIS events. The observed differences between the data and the simulation in these distributions result in errors on the prompt photon cross sections ranging from 10% to 20%.
- The uncertainties on the calorimeter electromagnetic and hadronic energy scales (0.7% to 1.5% and $\approx 3\%$ respectively) contribute errors of about 5% for the inclusive cross sections. For the case with associated jets, the hadronic energy uncertainty gives rise to uncertainties of about 10%.
- The trigger efficiency is determined using independent triggers with an uncertainty of 3%.
- The model dependence, of the corrections for detector effects is quantified as half the difference ($< 6\%$ in most cases) between the correction factors obtained with PYTHIA and HERWIG. Within these uncertainties the results are insensitive to reasonable variations of the E_T^γ dependence and of the underlying event activity in PYTHIA.

An overall normalisation uncertainty of 1.5% on the luminosity measurement is not included in the results. The total systematic errors are obtained by adding the different systematic errors in quadrature. For further details see [14].

7 Results

The results are presented in Tables 1 to 3 and Figs. 3 to 6 as bin averaged ep cross sections in the kinematic region

[4] PYTHIA 6.15/70 and HERWIG 6.1 are used with default multiple interactions (MSTP(82)=1 for PYTHIA, PRSOF=1, BTCLM=1 for HERWIG).

Table 1. Inclusive prompt photon differential cross sections $d\sigma/dE_T^\gamma$ for $-1 < \eta^\gamma < 0.9$ and $d\sigma/d\eta^\gamma$ for $5 < E_T^\gamma < 10\,\text{GeV}$ with $\sqrt{s} = 319\,\text{GeV}$ and $0.2 < y < 0.7$. The first error is statistical, the second systematic. The correction factors applied to the NLO calculations for hadronisation and multiple interactions (h.c. + m.i.) are also given

E_T^γ (GeV)	$d\sigma/dE_T^\gamma$ (pb/GeV)	h.c.+ m.i
5.0–5.8	17.0 ±1.8± 2.9	0.75
5.8–6.7	11.6 ±1.2± 1.9	0.78
6.7–7.5	8.3 ±0.9± 1.3	0.84
7.5–8.3	6.67 ±0.69± 0.85	0.88
8.3–9.2	5.46 ±0.55± 0.93	0.91
9.2–10.0	2.42 ±0.48± 0.57	0.91
η^γ	$d\sigma/d\eta^\gamma$ (pb)	h.c.+ m.i.
−1.0–−0.7	26.8 ±2.6± 4.2	0.94
−0.7–−0.4	29.1 ±3.4± 5.2	0.87
−0.4–0.0	26.9 ±3.0± 4.3	0.84
0.0–0.3	24.7 ±2.7± 3.4	0.75
0.3–0.6	21.2 ±1.9± 3.5	0.71
0.6–0.9	11.0 ±1.6± 2.2	0.65

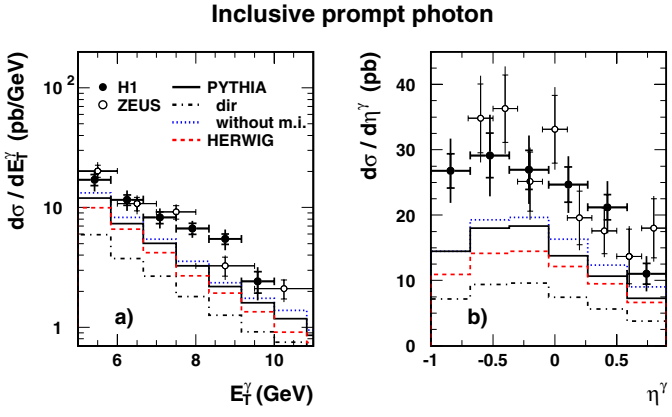

Fig. 3. Inclusive prompt photon differential cross sections $d\sigma/dE_T^\gamma$ for $-1 < \eta^\gamma < 0.9$ **a** and $d\sigma/d\eta^\gamma$ for $5 < E_T^\gamma < 10\,\text{GeV}$ with $\sqrt{s} = 319\,\text{GeV}$ and $0.2 < y < 0.7$ **b** compared with the predictions of HERWIG (dashed line) and PYTHIA including multiple interactions (full line). The contribution of direct interactions is shown separately (dashed-dotted line). The full PYTHIA prediction without multiple interactions (dotted line) is also shown. ZEUS data [2] are shown adjusted to correspond to $\sqrt{s} = 319\,\text{GeV}$, $0.2 < y < 0.7$ and $-1 < \eta^\gamma < 0.9$

defined by

$$\sqrt{s} = 319\,\text{GeV}\,, \quad 0.2 < y < 0.7\,, \quad Q^2 < 1\,\text{GeV}^2$$

and

$$5 < E_T^\gamma < 10\,\text{GeV}\,, \quad -1 < \eta^\gamma < 0.9\,, \quad E_T^{\text{cone}} < 0.1 \cdot E_T^\gamma\,.$$

The inner error bars on the data points in the figures indicate the statistical errors as obtained from the shower discriminating fits. The full error bars also contain the systematic errors added in quadrature.

Table 2. Prompt photon cross sections with an additional jet requirement ($E_T^{\text{jet}} > 4.5\,\text{GeV}$, $-1 < \eta^{\text{jet}} < 2.3$) differential in E_T^γ, η^γ, E_T^{jet}, η^{jet}, x_γ^{LO} and x_p^{LO} for $-1 < \eta^\gamma < 0.9$ and $5 < E_T^\gamma < 10\,\text{GeV}$ with $\sqrt{s} = 319\,\text{GeV}$ and $0.2 < y < 0.7$. The first error is statistical, the second systematic. The correction factors applied to the NLO calculations for hadronisation and multiple interactions (h.c. + m.i.) are also given

E_T^γ (GeV)	$d\sigma/dE_T^\gamma$ (pb/GeV)	h.c.+ m.i
5.0–5.8	8.9 ±1.2± 2.4	0.77
5.8–6.7	6.24 ±0.90± 1.02	0.80
6.7–7.5	6.10 ±0.77± 0.97	0.85
7.5–8.3	5.28 ±0.64± 0.71	0.89
8.3–9.2	3.98 ±0.51± 0.71	0.93
9.2–10.0	2.30 ±0.48± 0.52	0.91
η^γ	$d\sigma/d\eta^\gamma$ (pb)	h.c.+ m.i.
−1.0–−0.7	16.2 ±2.1± 2.8	0.95
−0.7–−0.4	18.2 ±2.5± 3.2	0.89
−0.4–0.0	18.2 ±2.4± 2.9	0.87
0.0–0.3	13.7 ±2.0± 2.2	0.77
0.3–0.6	14.5 ±1.5± 2.6	0.76
0.6–0.9	6.8 ±1.3± 1.6	0.71
E_T^{jet} (GeV)	$d\sigma/dE_T^{\text{jet}}$ (pb/GeV)	h.c.+ m.i.
4.5–6.7	5.97 ±0.54± 0.91	0.82
6.7–8.8	3.92 ±0.42± 0.72	0.84
8.8–11.0	2.07 ±0.26± 0.44	0.83
η^{jet}	$d\sigma/d\eta^{\text{jet}}$ (pb)	h.c.+ m.i.
−1.0–−0.3	7.5 ±1.2± 1.4	0.77
−0.3–0.3	12.4 ±1.2± 1.6	0.88
0.3–1.0	12.3 ±1.3± 2.0	0.86
1.0–1.6	6.58 ±0.87± 1.10	0.78
1.6–2.3	2.81 ±1.01± 0.94	0.91
x_γ^{LO}	$d\sigma/dx_\gamma^{\text{LO}}$ (pb)	h.c.+ m.i.
0.1–0.3	7.8 ±2.2± 2.5	0.50
0.3–0.6	16.4 ±2.8± 2.6	0.65
0.6–0.9	39.9 ±4.1± 7.4	1.1
0.9–1.1	49.3 ±4.1± 7.4	0.88
x_p^{LO}	$d\sigma/dx_p^{\text{LO}}$ (pb)	h.c.+ m.i.
0.0018–0.0034	247 ±149± 51	0.84
0.0034–0.0063	2350 ±300± 350	0.80
0.0063–0.0120	1900 ±180± 290	0.86
0.0120–0.0220	640 ±70± 113	0.81
0.0220–0.0400	167 ±31± 39	0.84

7.1 Inclusive prompt photons

Differential cross sections $d\sigma/dE_T^\gamma$ and $d\sigma/d\eta^\gamma$ for inclusive prompt photon production are shown in Fig. 3 and are compared with the predictions of the PYTHIA [10] and HERWIG [11] event generators. The cross sections are reasonably described in shape, but the predictions by PYTHIA (HERWIG) are low by about 40% (50%) in normalisation. Photons from fragmentation in di-jet events are only treated in the PYTHIA calculation, which explains the difference from HERWIG. The figure shows the full

Table 3. Normalised cross sections differential in the prompt photon momentum component perpendicular to the jet direction in the transverse plane, for $x_\gamma^{\rm LO} < 0.85$ and $x_\gamma^{\rm LO} > 0.85$ with $5 < E_T^\gamma < 10\,\text{GeV}$, $-1 < \eta^\gamma < 0.9$, $E_T^{\rm jet} > 4.5\,\text{GeV}$ and $-1 < \eta^{\rm jet} < 2.3$ with $\sqrt{s} = 319\,\text{GeV}$ and $0.2 < y < 0.7$. The first error is statistical, the second systematic

$p_\perp$ (GeV)	$1/\sigma\ \mathrm{d}\sigma/\mathrm{d}p_\perp(\text{GeV}^{-1})$, $x_\gamma^{\rm LO} < 0.85$
0–2	0.216 ±0.030± 0.015
2–4	0.117 ±0.022± 0.011
4–6	0.124 ±0.019± 0.011
6–8	0.0225 ±0.0081± 0.0077
$p_\perp$ (GeV)	$1/\sigma\ \mathrm{d}\sigma/\mathrm{d}p_\perp(\text{GeV}^{-1})$, $x_\gamma^{\rm LO} > 0.85$
0–2	0.420 ±0.033± 0.024
2–4	0.061 ±0.017± 0.014
4–6	0.0054 ±0.0078± 0.0026

PYTHIA prediction and separately the contribution of direct photon interactions only. The PYTHIA prediction is also shown without multiple interactions. The predictions at $0 < \eta^\gamma < 0.9$ are about 25% higher without multiple interactions, showing that the cross section is reduced by the soft underlying event activity, as expected [6] due to the isolation cone condition $E_T^{\rm cone} = 0.1 \cdot E_T^\gamma$. Figure 3 also shows a comparison with the results of the ZEUS collaboration [2].[5] The two measurements are consistent.

The results are further compared in Figs. 4a,b with the NLO pQCD calculations by Fontannaz, Guillet and Heinrich (FGH) [6] and Krawczyk and Zembrzuski (K&Z) [8,9]. The two calculations are similar, the main difference being that only FGH apply higher order corrections to the resolved photon processes (Fig. 1c,d). The final state photon can be emitted in a hard partonic process or can be produced in the fragmentation of a quark or gluon. The photon isolation requirement in the cross section definition suppresses the latter contribution considerably. According to the calculations, the contribution to the cross sections from fragmentation is typically 10%. Both calculations use the photon and proton parton density functions AFG [20] and MRST2 [21], respectively, and BFG [22] fragmentation functions. The transverse energy E_T^γ is used for the renormalisation and factorisation scales. In order to obtain a realistic comparison of data and theory, the NLO calculations are shown after correction from the parton to the hadron level including the effects of multiple interactions (m.i.). These corrections are obtained using the average of PYTHIA and HERWIG, taking half the difference as an uncertainty estimate. The resulting uncertainty is typically 3% as shown by the outer error bands in Figs. 4a,b.

The FGH (K&Z) NLO calculations are typically 30% (40%) below the data in most of the E_T^γ and η^γ ranges presented in Figs. 4a,b, if the corrections for hadronisation and m.i. are applied. The comparison with the parton level result of FGH shows that the correction factors are largest

[5] The ZEUS data are obtained in the somewhat different kinematic region $0.2 < y < 0.9$, $-0.7 < \eta^\gamma < 0.9$, $\sqrt{s} = 301\,\text{GeV}$ and are adjusted to correspond to the H1 conditions using the NLO calculation [6].

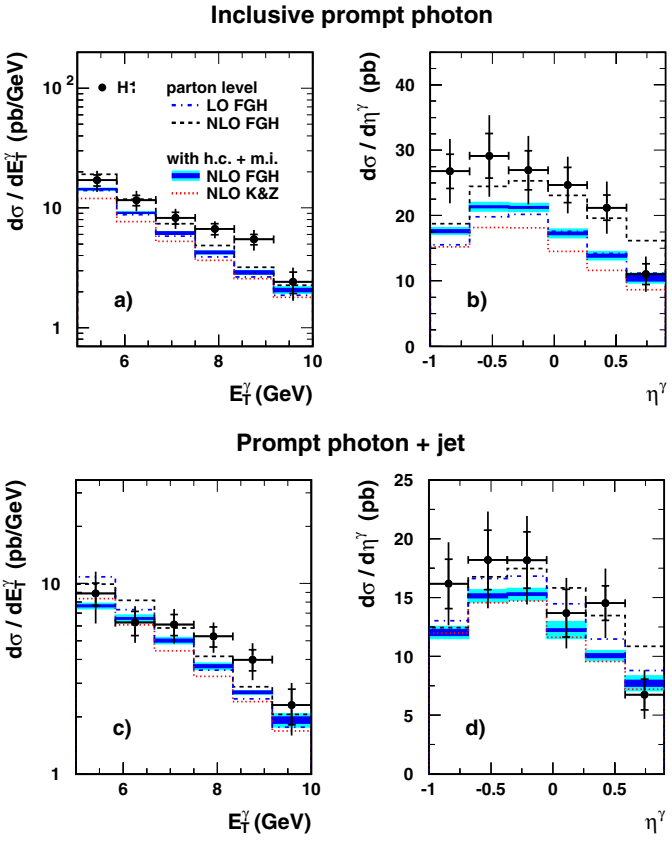

Fig. 4. Inclusive prompt photon cross sections **a,b** for $-1 < \eta^\gamma < 0.9$ and $5 < E_T^\gamma < 10\,\text{GeV}$ with $\sqrt{s} = 319\,\text{GeV}$ and $0.2 < y < 0.7$, and with an additional jet requirement ($E_T^{\rm jet} > 4.5\,\text{GeV}$, $-1 < \eta^{\rm jet} < 2.3$) **c,d**. The data are compared with NLO pQCD calculations (K&Z [9], dotted line, and FGH [6], solid line). The NLO results are corrected for hadronisation and multiple interaction (h.c. + m.i.) effects (see text). The outer error bands show the estimated uncertainties on these corrections for the example of FGH, added linearly to the effect of a variation of the renormalisation and factorisation scales in the NLO calculation from $0.5 \cdot E_T^\gamma$ to $2 \cdot E_T^\gamma$ (inner band). The FGH results are also shown without corrections for h.c. and m.i. at NLO (dashed) and LO (dashed-dotted)

at high η^γ, where resolved photon interactions contribute most. Only here ($\eta^\gamma > 0.6$) the corrections improve the agreement with the data. The NLO corrections are substantial, with the NLO/LO ratio increasing from 1.2 to 1.4 for FGH with increasing η^γ. The effect on the NLO calculations of scale variations is rather small as shown by the inner error bands in Fig. 4a,b, which indicates the effect of the variation of the renormalisation and factorisation scales from $0.5 \cdot E_T^\gamma$ to $2 \cdot E_T^\gamma$. The predictions are about 10% larger on average if the GRV parton density and fragmentation functions [19, 23] are used.

7.2 Prompt photons with jets

Cross sections for the production of a prompt photon associated with a jet are presented in Figs. 4c,d as a function of the variables E_T^γ and η^γ and in Fig. 5 as func-

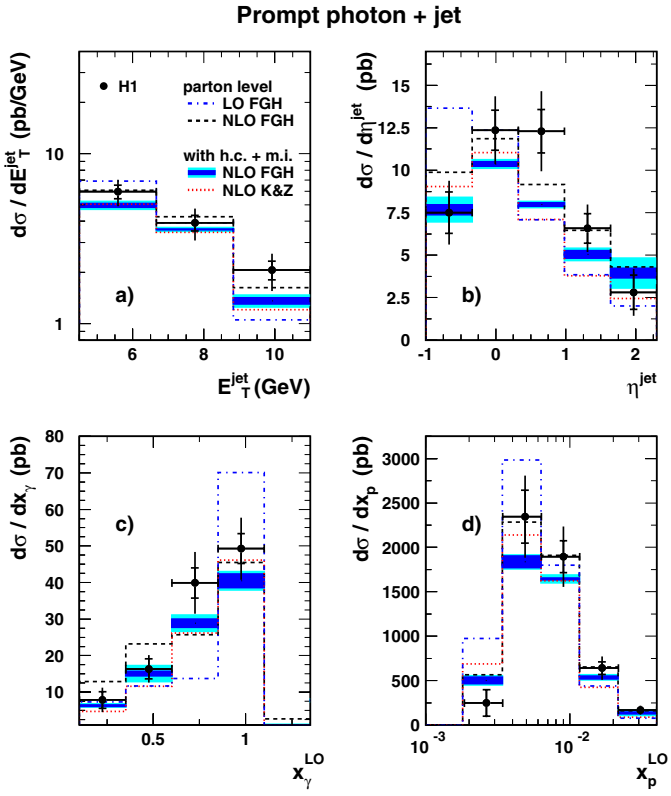

Fig. 5. Prompt photon cross sections with an additional jet requirement ($E_T^{\rm jet} > 4.5\,\text{GeV}$, $-1 < \eta^{\rm jet} < 2.3$) differential in $E_T^{\rm jet}$, $\eta^{\rm jet}$, $x_\gamma^{\rm LO}$ and $x_p^{\rm LO}$. The data are compared with NLO pQCD calculations (K&Z [9], dotted line and FGH [6,7] solid line). The NLO results are corrected for hadronisation and multiple interaction (h.c.+ m.i.) effects (see text). For the error bands see Fig. 4. The FGH results are also shown without corrections for h.c. and m.i. at NLO (dashed) and LO (dashed-dotted)

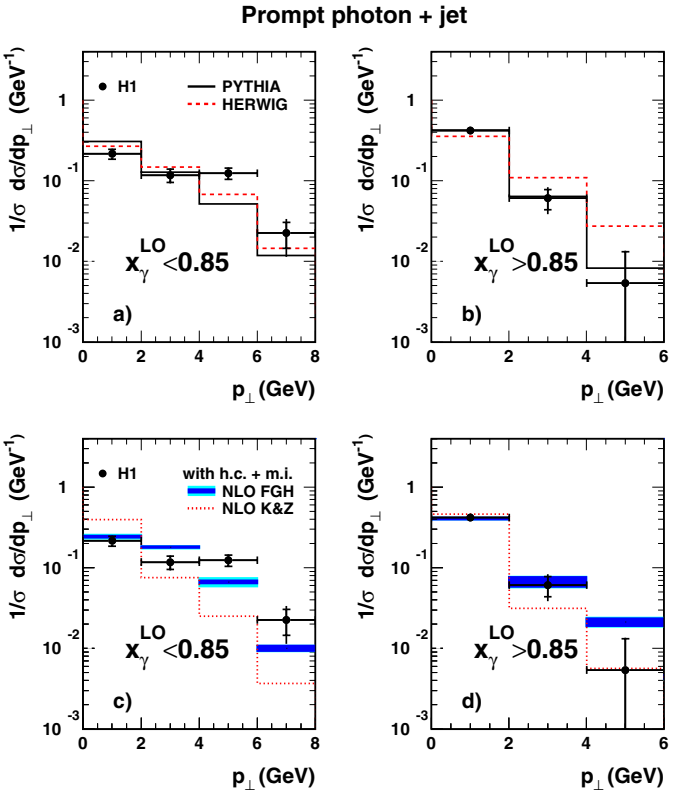

Fig. 6. Distribution of the prompt photon momentum component, perpendicular to the jet direction in the transverse plane, for $x_\gamma^{\rm LO} < 0.85$, **a** and **c**, and $x_\gamma^{\rm LO} > 0.85$, **b** and **d**. In **a** and **b** the data are compared with PYTHIA (solid line) and HERWIG (dashed line). In **c** and **d** the data are compared with NLO pQCD calculations (K&Z [9], dotted line, and FGH [6,7], solid line). The NLO results are corrected for hadronisation and multiple interactions. For the error bands see Fig. 4

tion of $E_T^{\rm jet}, \eta^{\rm jet}, x_\gamma^{\rm LO}$ and $x_p^{\rm LO}$. The estimators $x_\gamma^{\rm LO} = E_T^\gamma(e^{-\eta^{\rm jet}} + e^{-\eta^\gamma})/2yE_e$ and $x_p^{\rm LO} = E_T^\gamma(e^{\eta^{\rm jet}} + e^{\eta^\gamma})/2E_p$ are taken for the momentum fractions of constituents of the incident photon and proton, respectively, participating in the hard process. These observables use the photon energy in place of the more poorly reconstructed jet energy, such that hadronic energy measurements enter only through y. They are most easily interpreted in the leading order (LO) approximation where the outgoing partons from the hard interaction, and correspondingly the reconstructed photon and jet, have equal transverse momenta. The use of the variable $x_\gamma^{\rm LO}$ was recommended to reduce infrared sensitivity [7, 20]. The variable $x_p^{\rm LO}$ is discussed e.g. in [24].

The data are compared with the pQCD calculations. In contrast to the inclusive case, both NLO calculations are consistent with the data in most bins. The NLO/LO correction ratios for $\mathrm{d}\sigma/\mathrm{d}\eta^\gamma$ are more moderate than in the inclusive case, ranging from about 0.95 to 1.25 with increasing η^γ for FGH (Fig. 4d), but are still large in some bins of other distributions, as shown in Fig. 5. The hadronic and m.i. corrections, which are applied for both NLO calculations, improve the description of the data only in some regions, such as $\eta^\gamma > 0.6$, $\eta^{\rm jet} < -0.3$ and $x_\gamma^{\rm LO} < 0.6$. The $x_\gamma^{\rm LO}$ distribution (Fig. 5c) is particularly sensitive to the photon structure function. Using the GRV parameterisation [19, 23], the K&Z prediction increases by about 4% for $x_\gamma^{\rm LO} > 0.85$ and by about 20% at $x_\gamma^{\rm LO} < 0.85$ where resolved photon contributions dominate, leading to a somewhat improved description of the data.

Further understanding of the dynamics of the process and in particular of the effect of higher order gluon emissions beyond the diagrams shown in Fig. 1 may be obtained from the transverse correlation between the prompt photon and the jet. The distribution of the component of the prompt photon's momentum perpendicular to the jet direction in the transverse plane,

$$p_\perp \equiv |\mathbf{p}_T^\gamma \times \mathbf{p}_T^{\rm jet}|/|\mathbf{p}_T^{\rm jet}| = E_T^\gamma \cdot \sin(\Delta\phi)\,,$$

where $\Delta\phi$ is the difference in azimuth between the photon and the jet, is determined by higher order effects as $p_\perp$ is zero at leading order, where the prompt photon and the jet are back-to-back in the transverse plane.

The normalised $p_\perp$ distribution is shown in Fig. 6 separately for the regions $x_\gamma^{\rm LO} > 0.85$ and $x_\gamma^{\rm LO} < 0.85$, where

direct and resolved photon induced processes dominate, respectively (contributing about 80% in each case according to the FGH calculation). The FGH NLO prediction gives a better description of the $p_\perp$ distributions than K&Z. This is due, at least in part, to the differences between the QCD corrections for resolved photon interactions in the two calculations. For $x_\gamma^{\rm LO} > 0.85$, the data are quite well described by PYTHIA, whereas the HERWIG prediction is somewhat harder than that of the data. For $x_\gamma^{\rm LO} < 0.85$, the measured distribution is reasonably well described by both Monte Carlo models, except in the region of $p_\perp \approx 5\,\text{GeV}$. The $p_\perp$ distribution at large x^γ has previously been used [3] to extract information on an intrinsic k_t of the initial state partons of the proton. However, the large differences between the predictions of the various NLO calculations and Monte Carlo models in the present comparisons do not allow a reliable statement to be made.

8 Conclusions

The photoproduction of prompt photons, both inclusively and associated with jets, is studied. The measured η^γ and E_T^γ distributions of the inclusive prompt photons are reasonably well described in shape by NLO pQCD calculations, but after corrections for hadronisation and multiple interactions the predictions are $30\% - 40\%$ below the data. The cross sections predicted by the PYTHIA and HERWIG event generators describe the data distributions well in shape with normalisations that are low by about $40\% - 50\%$.

For prompt photons associated with a jet, the data are somewhat better described by the NLO calculations including corrections for hadronisation and multiple interactions. This, together with the fact that the NLO corrections are smaller on average than in the inclusive case, suggests that contributions beyond NLO are less important if an energetic jet is selected together with the prompt photon.

The distribution of $p_\perp$, the component of the prompt photon's momentum perpendicular to the jet direction in the transverse plane, is sensitive to effects beyond LO. The PYTHIA generator describes the normalised $p_\perp$ distributions quite well, whereas HERWIG predicts too hard a $p_\perp$ distribution at large $x_\gamma^{\rm LO}$, where direct photon interactions dominate. Particularly at low $x_\gamma^{\rm LO}$, the $p_\perp$ distribution is better described by the NLO calculations if NLO QCD corrections are also applied in the case of the resolved photon interactions.

Acknowledgements. We are grateful to the HERA machine group whose outstanding efforts have made this experiment possible. We thank the engineers and technicians for their work in constructing and maintaining the H1 detector, our funding agencies for financial support, the DESY technical staff for continual assistance and the DESY directorate for support and for the hospitality which they extend to the non DESY members of the collaboration. We are grateful to Gudrun Heinrich and Andrzej Zembrzuski for discussions and help with the NLO QCD calculations.

References

1. L. Apanasevich et al., Phys. Rev. D **59**, 074007 (1999) [hep-ph/9808467]; L. Apanasevich et al., Phys. Rev. D **63**, 014009 (2001) [hep-ph/0007191]; A. Kumar et al., Phys. Rev. D **68**, 014017 (2003); L. Apanasevich et al. [Fermilab E706 Collaboration], hep-ex/0407011.
2. J. Breitweg et al. [ZEUS Collaboration], Phys. Lett. B **472**, 175 (2000) [hep-ex/9910045].
3. S. Chekanov et al. [ZEUS Collaboration], Phys. Lett. B **511**, 19 (2001) [hep-ex/0104001].
4. H.L. Lai and H.n. Li, Phys. Rev. D **58**, 114020 (1998) [hep-ph/9802414]; M.A. Kimber, A.D. Martin and M.G. Ryskin, Eur. Phys. J. C **12**, 655 (2000) [hep-ph/9911379]; E. Laenen, G. Sterman and W. Vogelsang, Phys. Rev. Lett. **84**, 4296 (2000), [hep-ph/0002078]; Phys. Rev. D **63**, 114018 (2001), [hep-ph/0010080]; N. Kidonakis and J.F. Owens, Int. J. Mod. Phys. A **19**, 149 (2004) [hep-ph/0307352]; Phys. Rev. D **61**, 094004 (2000) [hep-ph/9912388].
5. L.E. Gordon and W. Vogelsang, Phys. Rev. D **52**, 58 (1995); L.E. Gordon, Phys. Rev. D **57**, 235 (1998) [hep-ph/9707464].
6. M. Fontannaz, J.P. Guillet and G. Heinrich, Eur. Phys. J. C **21**, 303 (2001) [hep-ph/0105121].
7. M. Fontannaz, J.P. Guillet and G. Heinrich, Eur. Phys. J. C **22**, 303 (2001) [hep-ph/0107262].
8. M. Krawczyk and A. Zembrzuski, Phys. Rev. D **64**, 114017 (2001) [hep-ph/0105166].
9. A. Zembrzuski and M. Krawczyk, Photoproduction of isolated photon and jet at the DESY HERA, IFT-2003-27 [hep-ph/0309308].
10. T. Sjöstrand, P. Edén, C. Friberg, L. Lönnblad, G. Miu, S. Mrenna and E. Norrbin, Comput. Phys. Commun. **135**, 238 (2001) [hep-ph/0010017].
11. G. Corcella et al., HERWIG 6.1 release note, hep-ph/9912396; G. Marchesini et al., Comput. Phys. Commun. **67**, 465 (1992).
12. B. Andrieu et al. [H1 Calorimeter Group], Nucl. Instrum. Meth. A **336**, 460 (1993).
13. I. Abt et al. [H1 Collaboration], Nucl. Instrum. Meth. A **386**, 310 (1997); ibid. A **386**, 348 (1997).
14. R. Lemrani, Ph.D. Thesis, Hamburg University, 2003, DESY-THESIS-2003-010, also available at http://www-h1.desy.de/publications/theses_list.html.
15. T. Nicholls et al. [H1 SPACAL Group], Nucl. Instrum. Meth. A **374**, 149 (1996).
16. J. Burger et al., Nucl. Instrum. Meth. A **279**, 217 (1989).
17. S.D. Ellis and D.E. Soper, Phys. Rev. D **48**, 3160 (1993) [hep-ph/9305266].
18. T. Sjöstrand, Comput. Phys. Commun. **82**, 74 (1994).
19. M. Glück, E. Reya and A. Vogt, Phys. Rev. D **46**, 1973 (1992); Z. Phys. C **67**, 433 (1995).
20. P. Aurenche, J.P. Guillet and M. Fontannaz, Z. Phys. C **64**, 621 (1994) [hep-ph/9406382].
21. A.D. Martin, R.G. Roberts, W.J. Stirling and R.S. Thorne, Eur. Phys. J. C **14**, 133 (2000) [hep-ph/9907231].
22. L. Bourhis, M. Fontannaz and J.P. Guillet, Eur. Phys. J. C **2**, 529 (1998) [hep-ph/9704447].
23. M. Glück, E. Reya and A. Vogt, Phys. Rev. D **45**, 3986 (1992); Phys. Rev. D **48**, 116 (1993) [Erratum-ibid. D **51**, 1427 (1995)].
24. M. Fontannaz, J.P. Guillet and G. Heinrich, Eur. Phys. J. C **26**, 209 (2002) [hep-ph/0206202]; G. Heinrich, IPPP-03-21 [hep-ph/0304158].